2003

An in situ Electrochemical Study of Electrodeposited Nickel and Nickel-Yttrium Oxide Composite Using Scanning Electrochemical Microscopy

David O. Wipf
Mississippi State University, dow1@msstate.edu

L. Diaz-Ballote

L. Veleva

An *in situ* Electrochemical Study of Electrodeposited Nickel and Nickel-Yttrium Oxide Composite Using Scanning Electrochemical Microscopy

L. Veleva[*a], L. Diaz-Ballote[a] and David O. Wipf[*z]

Department of Chemistry, Box 9573, Mississippi State University, Mississippi State, MS 39762, USA

ABSTRACT

Electrodeposited nickel and nickel-yttrium oxide composite samples were studied *in situ* using scanning electrochemical microscopy (SECM). The monitored probe currents in phosphate-citrate buffer (pH 4.2) in the presence or absence of $Ru(NH_3)_6^{3+}$ as an oxidizing mediator near the Ni surface show that the SECM is a useful tool for study of the electrochemical activity of heterogeneous metal surface at micrometer scales. The SECM ultramicroelectrode probe tip provides information about the shape, activity and location of particles, such as Y_2O_3 introduced (co-deposited) in the Ni-matrix of the composite. Experiments show that the Ni-matrix in the composite coating is more active than the pure Ni-coating. This fact is expected, because of texture changes in the Ni structure upon introduction (by co-deposition) of Y_2O_3 particles. In the absence of mediator in the solution, the electrochemical activity of heterogeneous metal surface at a micro-level is investigated by using O_2 concentration changes. The rate of reaction for O_2 reduction was found to locally vary at electrodes floating at the open-circuit potential (o.c.p) when compared to an electrode potentiostatically polarized at a more positive potential than the o.c.p. This behavior suggests that local anode and cathode regions are being observed at the o.c.p. sample.

Published as L. Veleva *et al* 2003 *J. Electrochem. Soc.* **150** C1
https://doi.org/10.1149/1.1522722

Submitted to the Journal of the Electrochemical Society. Feb. 28, 2002, revision submitted May XX, 2002

---

[*] Electrochemical Society Member
[a] Permanent address: Research Center for Advanced Study (CINVESTAV-IPN), Unidad Merida, Applied Physics Department, Carr. Ant. a Progreso Km.6, Cordemex 73, C.P. 97310, Merida, Yucatan, Mexico veleva@mda.cinvestav.mx or lveleva@hotmail.com
[z] wipf@ra.msstate.edu

Nickel coatings are widely used to protect iron, copper or zinc alloys against corrosive attack in rural or industrial atmosphere or are used as undercoating on brass and chromium for precious metals coatings.[1] Because nickel is magnetic, it is sometimes plated (electrodeposited) where magnetic properties are desired. Nickel can be deposited with minimal internal stress and is therefore useful in electroforming and aerospace applications. Nickel plating for engineering purposes provides relatively good wear and abrasion resistance (on molds, for example) and it is also used on electronic circuit boards as a protective barrier layer against corrosive chemical environments. In several applications, nickel composites have been formed where the nickel is co-deposited with dispersed inert inorganic particles such as RuO_2, SiO_2 and SiC. [2-4] Lately, the use and deposition of yttrium-oxide thin films, as well as complex metal-oxide films containing Y_2O_3 are of interest for electrochemical and electronic applications.[5-7]

Sintered yttrium oxide (Y_2O_3) is a white polycrystalline powder, with a high melting temperature (2400 °C), high breakdown mechanical strength, and good chemical stability. It has weakly alkaline properties and is only slightly soluble in water (pH ≅ 7), forming $Y(OH)_3$. The oxide is insoluble in alkaline solutions but is more soluble in acid pH, producing salts, which are hydrolyzed in several steps, giving various positively charged cations, as shown in equation 1:

$$[Y(H_2O)_6]^{3+} \rightarrow [Y(H_2O)_5OH]^{2+} \rightarrow [Y(H_2O)_4(OH)_2]^{+} \rightarrow \ldots . \qquad [1]$$

The solubility of yttrium oxide is highest at pH < 1.5 but undergoes hydrolysis at pH > 2. The probable crystal structure of Y_2O_3 indicates spatial composition inhomogeneity, with the presence of oxygen vacancies, the presence of defects, and an evolution of the covalent bond Y-O.[8 9]

A simple Ni-Cr matrix, when combined with the strengthening effect of Y_2O_3 dispersoid during mechanical alloys, provides excellent creep properties and resistance to thermal fatigue. In addition, chemical surface resistance is improved and operation in severe conditions (industrial environments) without protective coatings is possible.[10] Similar effects and improvement of the corrosion resistance were found for a zirconium matrix, due to the addition of Y_2O_3 dispersoid[11] and for Zn-Al-Cu alloy, modified by deposition of a thin layer of Y_2O_3.[12,13]

In our previous study,[14] solid particles of Y_2O_3 were co-deposited in a matrix of plated Ni, (from a Watts bath) and this composite was compared to pure plated Ni. Some differences in the electrochemical behavior of both coatings were detected in polarization curve, cyclic voltammetry, and impedance (EIS) measurements. Changes in corrosion-current density, polarization resistance, and charge-current density were probably due to the blocking effect of Y_2O_3 particles at the composite surface. Correcting for the actual metal area was difficult because the clusters of Y_2O_3 are not distributed uniformly within the Ni-composite matrix and the particle diameter ranges from 0.5 to 10 μm. Thus, the previously measured parameters produce an average electrochemical response over the entire composite area and, due to this fact, information about the local activity of nickel near and far from the Y_2O_3 particles is lost.

The scanning electrochemical microscope (SECM)[15] is used here to provide local information about the electrochemical activity of the nickel/nickel composite surfaces. The SECM uses an ultramicroelectrode (UME) probe, with a diameter of a few nm to 25 μm, to image topographic and chemical variations near a phase surface. This information can be used to examine different local electrochemical activities.[16-24] For example,

images of surface reactivity are obtained by moving the UME probe parallel to a sample's surface at a constant distance (a few tip diameters). Since this method does not require electrical contact with the sample, there are few restrictions on the chemical or physical nature of the sample. The *feedback mode* of the SECM uses a mediator species to provide information about the electrochemical activity (with respect to the mediator species) of the substrate.[25] The feedback experiment uses the probe tip electrode to generate an oxidized or reduced form of the mediator. At close probe-substrate separation, the mediator can quickly diffuse to the substrate surface. *"Positive" feedback* occurs if the mediator is returned to its original oxidation state by electron-transfer at the substrate. The probe current increases during positive feedback due to the regeneration process. The increase in current is a function of the probe-substrate separation and the rate of substrate-mediator electron transfer. *"Negative" feedback* occurs at an inert substrate. The probe current decreases as the probe-substrate separation decreases due to diffusional blocking of the substrate surface. An alternate experiment uses the probe as a scanning electrochemical sensor. In the *substrate generation/tip collection* (SG/TC)[26] mode the probe senses the concentration of redox-active species generated at the substrate surface.[27,28] Here, the probe is an amperometric electrode and the signal at the tip is, in principle, proportional to the concentration of redox active species in solution. The SG/TC is more sensitive to concentration changes than the feedback mode. Conversely, diffusion and convection cause the concentration of redox species to extend significantly beyond the source, which makes the spatial resolution in SG/TC mode less than feedback mode.

In this paper, both feedback and SG/TC modes of the SECM are used to examine and compare the local chemical activity of nickel and nickel-Y_2O_3 composite electrodes:

firstly, by addition of a mediator and then by examination of local O_2 concentration near the sample surface.

Experimental

Electrochemical Deposition of Nickel and Nickel-Y_2O_3 Composite Deposition occurred in a classical Watts bath containing (g/l): 250 $NiSO_4 \cdot 7H_2O$, 60 $NiCl_2 \cdot 6H_2O$, and 35 H_3BO_3 (analytical reagent chemicals) at pH 3.5 - 4.2. The experiment was performed at 55 °C and 4 A/dm^2 current density (galvanostatic mode) on a stainless steel cathode, which allowed a later removal of the Ni coating for testing. The substrate was mechanically polished, etched, and degreased before deposition of each coating. Two Ni anodes (99.99 %) were arranged on either side of the cathode to produce a homogeneous electric field. For the composite electrodeposition, 50-70 g/l Y_2O_3 powder, with particle diameter less than 0.5 μm, (produced by the Institute for Pure Compounds of Bulgaria) was introduced into the bath. Particles were held in suspension by air bubble agitation from the bottom of the bath cell.

The co-deposition conditions for Y_2O_3 are such that the solid oxide particles (or their hydrated complex) are positively charged because the solution pH is lower than their isoelectric point (i.e.p. ~ pH 7.6).[29,30] In addition, hydrolysis of Y_2O_3 (eq. 1) also leads to cationic particles. The Y_2O_3 particles are thus attracted and adhere to (adsorb) on the negatively charged cathode. Under these conditions, Y_2O_3 is embedded in the growing metal layer of Ni.

Stripped coating samples were evaluated by means of a scanning electron microscope (SEM) and energy dispersive X-ray analyzer (EDX), to explore morphology

and composition, respectively. It can be seen (Fig. 1) that the dark particles of Y_2O_3 have been incorporated in the Ni matrix as individual particles or, more often, as clusters with diameter greater than 2-3 μm. The EDX microanalysis confirmed the presence of a significant amount of yttrium in the composite, especially compared to the Ni coating (Figs. 2-3).

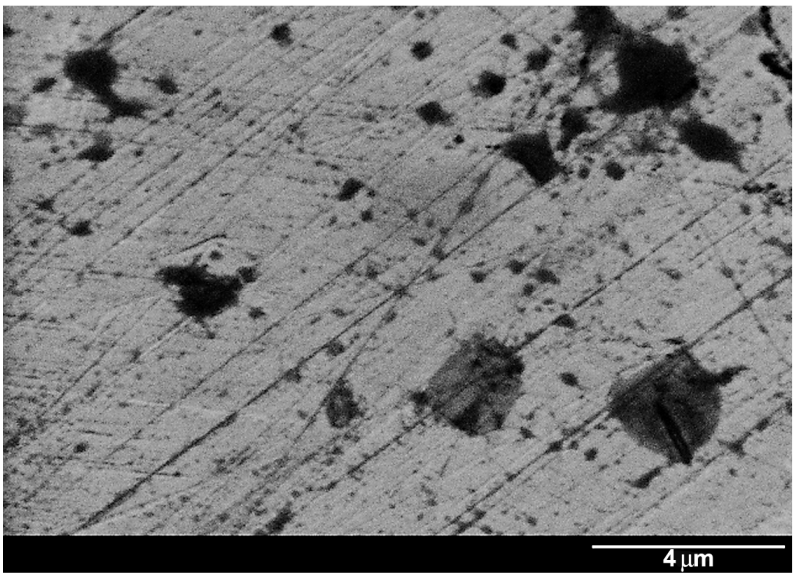

Fig.1 Cross-sectional SEM image of electrodeposited Ni-Y_2O_3 composite coating. The black color spots and stains represent yttrium oxide particles and their clusters (aggregations).

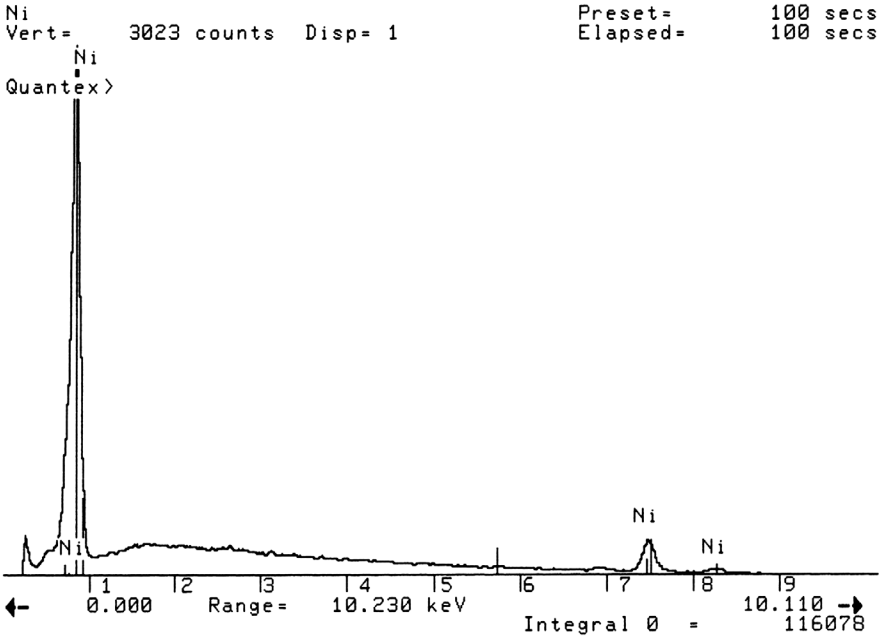

Fig. 2 EDX spectra of electrodeposited Ni coating.

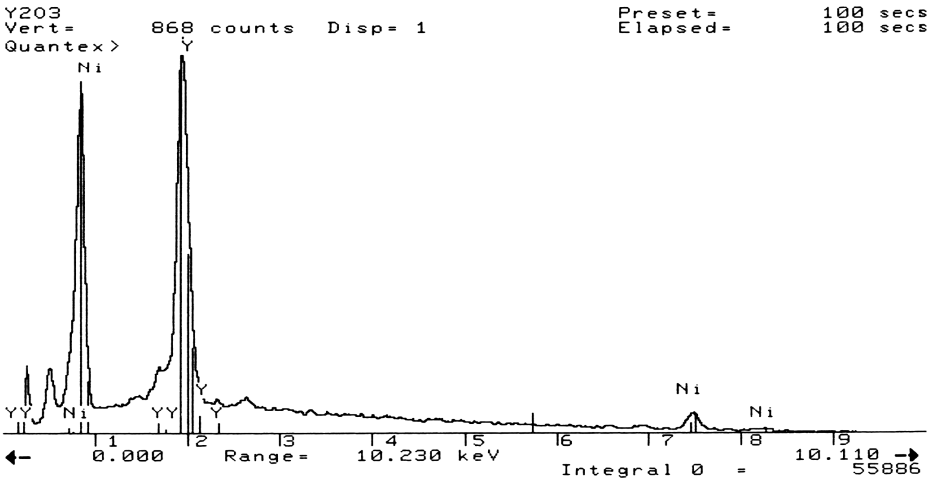

Fig. 3 EDX spectra of electrodeposited Ni-Y_2O_3 composite coating.

SECM Experiments The SECM images were obtained by scanning the probe (a 2-μm-diameter Pt tip) parallel to the cross section of the Ni coatings (electrodeposited Ni and Ni-composite). The experimental setup is similar to that previously reported.[25,31-33] The probe is mounted on a TS-75Z stage with integral encoder (Burleigh, Instruments, Inc.) for vertical movement. TSE-150 translation stages were used for horizontal movement. Closed-loop positioning was accomplished with a Burleigh 6000 ULN controller. An EI-400 bipotentiostat (Ensman Instrumentation) was used for all SECM experiments. Data acquisition and position control were enabled with a custom LabView (National Instruments, Austin, TX) program. Samples of the Ni and Ni-Y_2O_3 were embedded in epoxy and polished to expose a cross-section composite (60-80 μm thick of 2-3 mm long sample) of the composite material for imaging. Before all experiments, samples were polished with 0.05 μm gamma alumina powder (Buehler Inc.). All potentials are referenced to a Ag/AgCl electrode.

The electrochemical study was performed in two solutions: a pH 4.2 phosphate-citrate buffer[34] with 2 mM $Ru(NH_3)_6^{3+}$ (as $(Ru(NH_3)_6Cl_3$) as a mediator (oxidizing agent) and a pH 4.2 phosphate-citrate buffer with 6 mM NaCl (to replace the chloride anions that are introduced by dissociation of the ruthenium salt). This pH buffer was chosen because it approximates an acid, polluted atmospheric environment, in absence or presence of chloride contamination (in coastal regions). All SECM experiments were performed at an initial probe-substrate separation of about 2-3 μm. This position was set by monitoring the probe current-distance curve or by carefully approaching the surface until electrical contact was detected between the probe and sample. During image acquisition, the probe scan-rate was normally 20 μm/s.

Results and Discussion

SECM in the Presence of $Ru(NH_3)_6^{3+}$ Mediator Cyclic voltammetry on the Pt-tip (UME) showed that the half-wave reduction potential for the $Ru(NH_3)_6^{3+}/Ru(NH_3)_6^{2+}$ couple is about –0.175 V (vs. Ag/AgCl) in pH 4.2 phosphate-citrate buffer. The open-circuit potentials (o.c.p.) of the Ni and Ni-Y_2O_3 composites in this solution are –0.20 V and –0.21 V (vs. Ag/AgCl), respectively. Since the open circuit substrate reduces $Ru(NH_3)_6^{3+}$ to $Ru(NH_3)_6^{2+}$, a *substrate generation-tip collection* (SG/TC) SECM experiment was used, in which the substrate was held at o.c.p. during the SECM experiment and the probe potential was –0.05 V to oxidize (collect) the substrate generated $Ru(NH_3)_6^{2+}$. The probe current, thus, is a concentration map of the $Ru(NH_3)_6^{2+}$ near the metal substrate. Depending on the substrate activity, the reduction of $Ru(NH_3)_6^{3+}$ will occur at a higher or lower rate, producing a higher or lower concentration of this ion. Some contribution due to feedback of the $Ru(NH_3)_6^{3+}/Ru(NH_3)_6^{2+}$ is also expected given the substrate potential.

An SECM image of the probe current monitored at a 2-3 μm separation from the Ni-coating is presented in Fig. 4. The probe current is uniform over the Ni coating surface with an increase along the right edge of the Ni electrode. The increase can be ascribed to a slight tilt in the sample along both the right-left and top-bottom axes and also to the Ni protruding from the epoxy. The tip is closest to the surface at the top right. The smooth, featureless image indicates that the reduction of $Ru(NH_3)_6^{3+}$ on the Ni coating occurs at about the same rate over the surface. The Ni-epoxy boundary is sharply defined by a 3-4 fold lower probe current ($Ru(NH_3)_6^{2+}$concentration). The low concentration of $Ru(NH_3)_6^{2+}$ over the epoxy substrate indicates that the epoxy is electrochemically inert.

Areas of the Ni-Y_2O_3 composite substrate containing a high concentration of Y_2O_3 particles were selected by optical microscopy (Fig. 5) for SECM imaging. The SECM image in Fig. 6 of Ni-Y_2O_3 composite substrate clearly indicates the shape and location of the larger Y_2O_3 particles. Smaller particles are not resolved but appear as slightly darker regions in the image. The concentration of $Ru(NH_3)_6^{2+}$ is very low over the oxide particles, indicating that $Ru(NH_3)_6^{2+}$ is produced principally on the Ni-matrix. Based on the overall probe current in Fig. 4 and Fig. 6, the composite Ni-matrix appears more active than the Ni-coating. This fact could be due to changes in the Ni structure because of the inclusion of Y_2O_3 particles in the Ni-matrix during the metal electrodeposition (such as the preferred orientation of its crystal planes, defects and internal stresses). The greater activity is also predicted by the more negative o.c.p. of the composite.

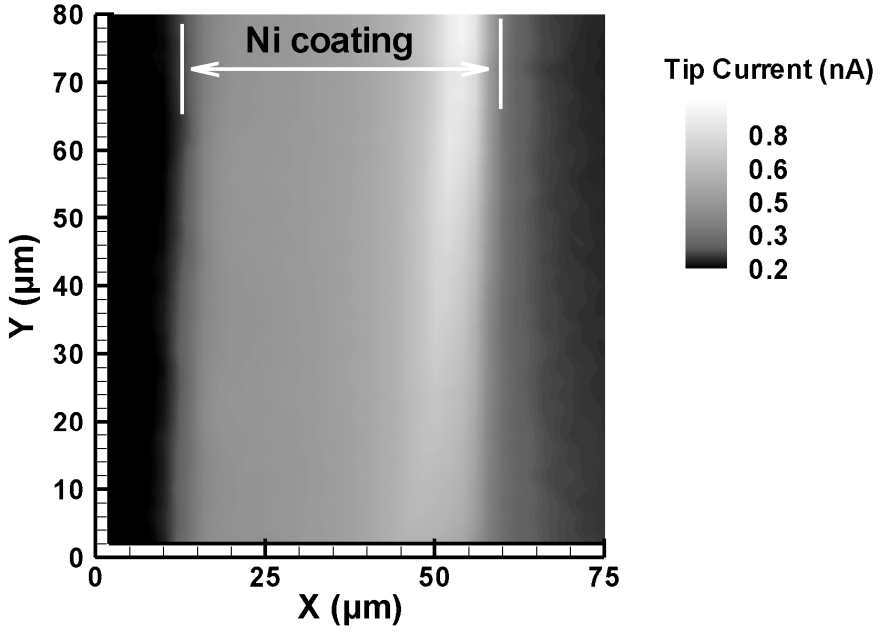

Fig. 4 SECM image of the probe current monitored on Ni coating (at o.c.p.). Scanned *in situ* in pH 4.2 phosphate-citrate buffer with 2.0 mM $Ru(NH_3)_6^{3+}$.

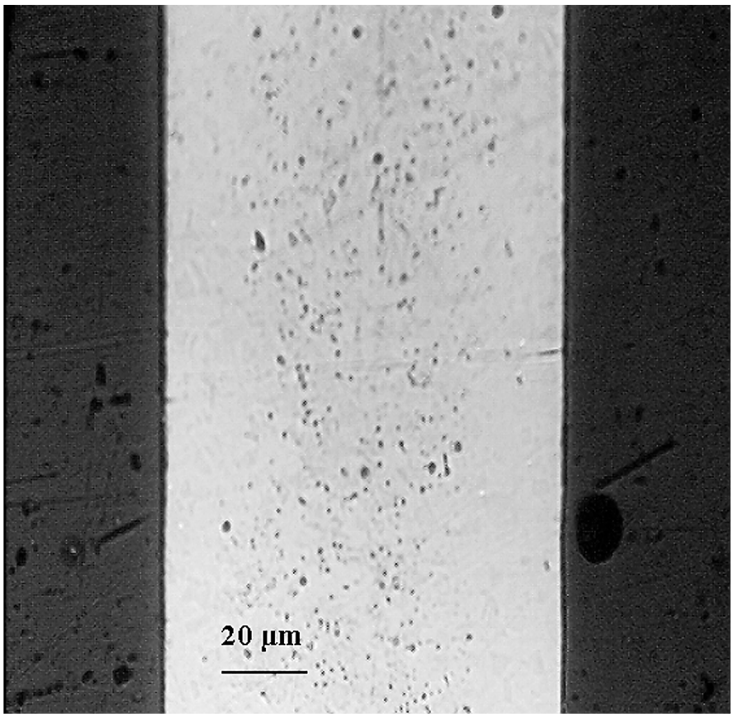

Fig. 5 Optical microscope image of Ni-Y_2O_3 composite substrate. (The black spots are Y_2O_3 particles).

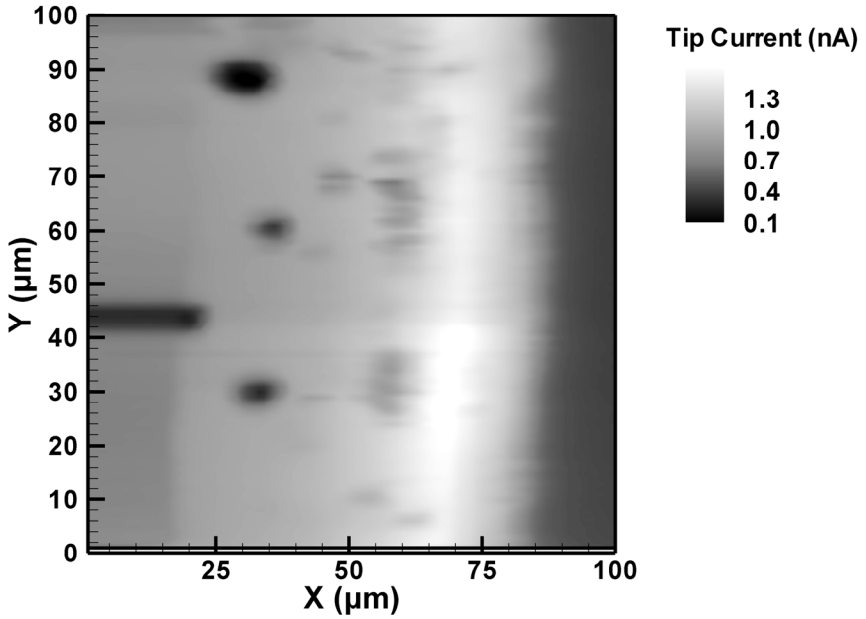

Fig. 6 SECM image of the probe current monitored on Ni-Y_2O_3 composite substrate (at o.c.p.). Scanned *in situ* in pH 4.2 phosphate-citrate buffer with 2.0 mM $Ru(NH_3)_6^{3+}$.

The SECM can also provide a vertical concentration map over the substrate. Rather than scan laterally at a fixed vertical position across a surface, the scan proceeds laterally along one axis and vertically along the other. An *x*-*z* vertical concentration map was acquired at the 50 μm *y* position of Fig. 6. Data were acquired by repetitive scans of 50 μm vertically from the electrode surface into the bulk solution while incrementing the *x* position. The monitored probe current is presented in Fig. 7. It shows how the "cloud" of $Ru(NH_3)_6^{2+}$ (formed on the Ni) increases, when the distance (axis *z*) between probe and Ni-composite surface decreases. (The dark areas in this SECM image, those with a lower probe current at left and right parts of axis *x*, represent epoxy substrate).

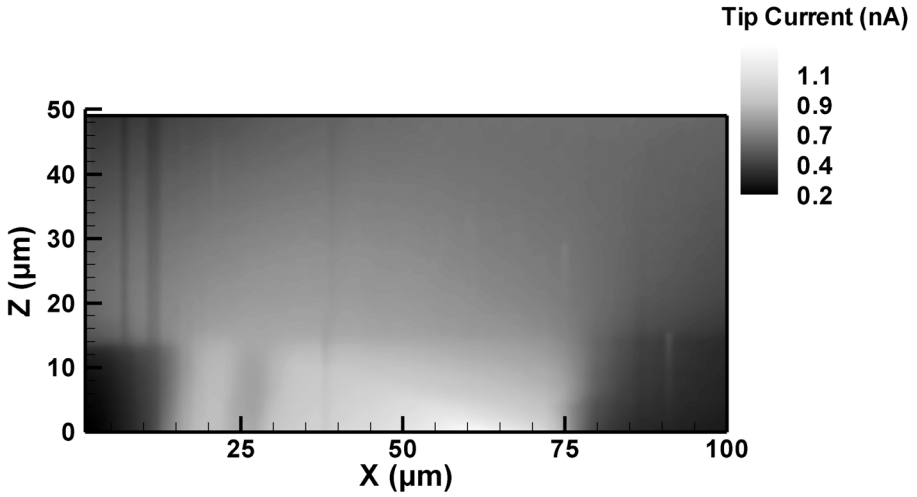

Fig. 7 SECM vertical concentration map showing the reduction current for $Ru(NH_3)_6^{3+}$. Acquired at a Ni-Y_2O_3 composite substrate in phosphate-citrate buffer at pH 4.2

Phosphate-Citrate Buffer with 6 mM NaCl $Ru(NH_3)_6^{3+}$ is a mild oxidizing agent and its presence during SECM experiments may accelerate corrosion of the Ni substrate. Eliminating the $Ru(NH_3)_6^{3+}$ mediator provides a more realistic view of the activity of the Ni or Ni-composite surface. According to the Pourbaix diagram for the electrochemical

equilibrium of Ni in aqueous solution,[35] at pH 4.2 and at a potential of -0.21 V (o.c.p.), nickel will be oxidized according to the reaction

$$Ni \rightleftharpoons Ni^{2+} + 2e^- \quad [2]$$

The pH and o.c.p. correspond to an area of the diagram in which water is stable and hydrogen evolution is not favored and, therefore, the corresponding reduction reaction is likely dissolved oxygen. The relevant half reaction in this buffered solution is

$$O_2 + 4H^+ + 4e^- \rightleftharpoons 2H_2O \quad [3]$$

Imaging of the O_2 concentration (consumed during the cathodic reaction on Ni) with the SECM gives an estimation by proxy of the Ni^{2+} formation at the substrate (the anodic reaction). A voltammogram at the probe electrode in this buffer solution shows a wave for oxygen reduction and its disappearance upon N_2 sparging (Fig. 8). Images were acquired by holding the probe electrode at a potential of –0.3 V in order to reduce O_2 (Fig. 8), while the Ni or Ni-composite substrate was unbiased and was floating at the o.c.p. The experiment in this case is a mixture of a negative feedback and a SG/TC experiment. Neither the tip nor substrate potential is sufficient to effect a mass-transfer limited reduction of O_2 (the substrate o.c.p. varied slightly between experiments but was always about –0.21 V vs. Ag/AgCl). This allows the tip to sample the O_2 concentration without significantly perturbing it through the electrolysis process. However, as the activity (the dissolution) of the Ni electrode changes, the concentration of the naturally present mediator (O_2) will be changed at the Ni surface.

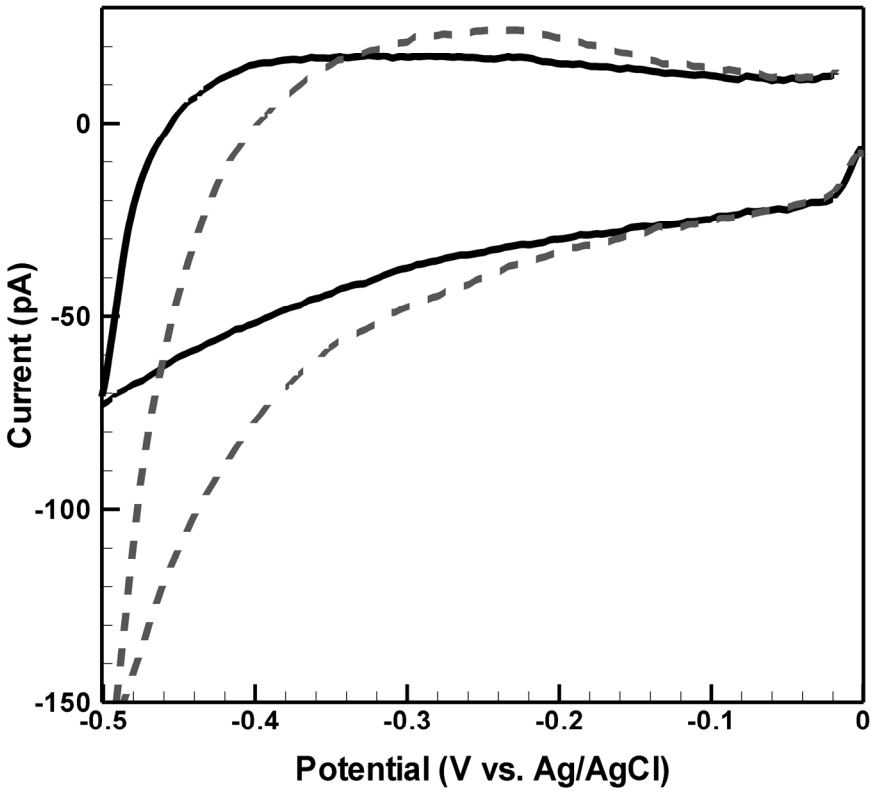

Fig. 8 Cyclic voltammogram (100 mV/s) at the probe (Pt UME) used in the SECM experiment, run in phosphate-citrate buffer at pH 4.2. (- - -) solution exposed to air, (——) solution deaerated with N_2 for 30 min.

Evidence for differences in the surface activity were found when the probe was scanned in the vicinity of Ni-Y_2O_3 composite substrate (Fig. 9). In this case, the O_2 reduction current is very small and the SECM image does not sharply define the shape of the Y_2O_3 particles or the metal-epoxy boundary. The dark region along the mid right indicates higher O_2 concentration at the edge of the composite and, thus, a likely region of high Ni dissolution. In addition several dark spots in the upper middle are likely at the location of Y_2O_3 particles. Over the Ni-composite substrate, O_2 is consumed (eq. 3) to support the Ni dissolution and the probe current is two-times smaller than that over the

epoxy substrate or Y_2O_3, where O_2 reduction does not occur. A corresponding SECM image at the Ni substrate is presented in Fig. 10A. The O_2 reduction current is also very low and in the same range as on Ni-composite.

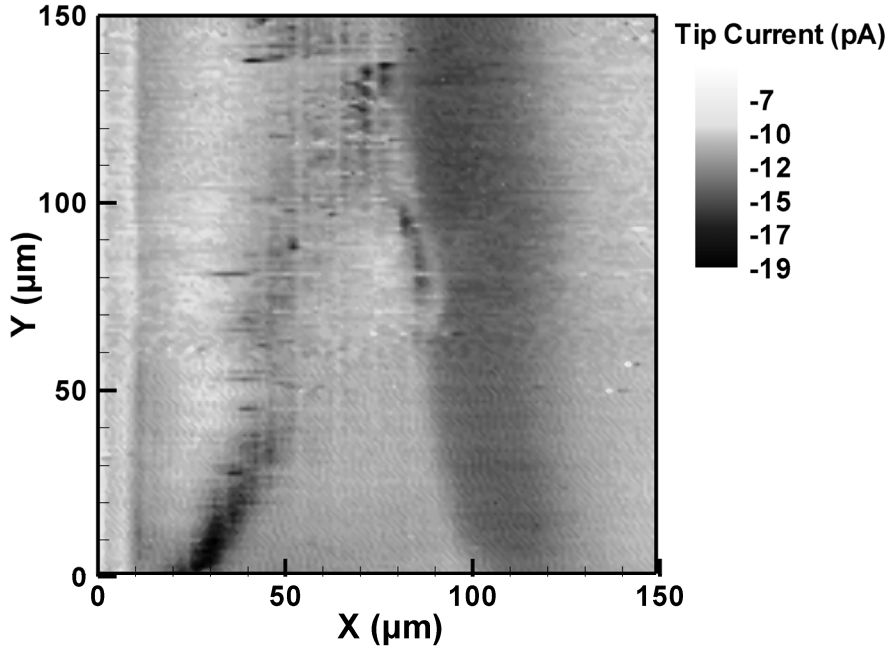

Fig. 9 SECM image of the probe current monitored on Ni-Y_2O_3 composite substrate (at o.c.p.), in phosphate-citrate buffer at pH 4.2

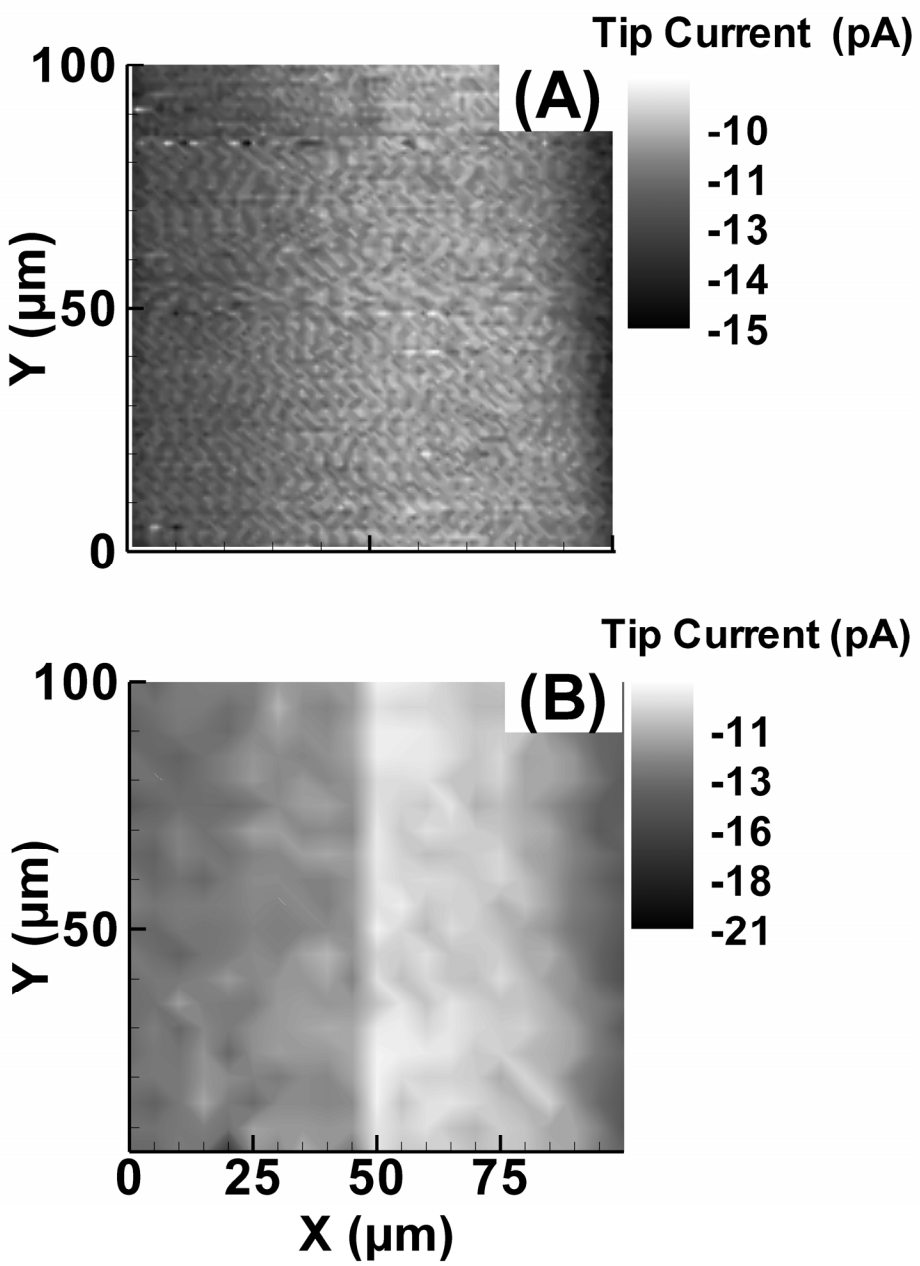

Fig. 10 SECM image of the probe current monitored on Ni-coating substrate. Scanned *in situ* in pH 4.2 phosphate-citrate buffer. (A) at o.c.p. and (B) at anodic polarization of 100 mV (vs. o.c.p.).

Applying an anodic polarization (100 mV vs. o.c.p.) at Ni (Fig. 10B) or Ni-composite (Fig. 11) accelerates the nickel dissolution in this buffer solution (in the presence of free chloride ions). For example, Fig. 11 presents the SECM image for the probe reduction current of oxygen found in a vicinity of Ni-composite. This figure is interesting in that it shows the evolution of the chemical environment as the substrate potential is moved from the o.c.p. to +100 mV of o.c.p. Acquiring a raster image requires a fixed amount of time and thus the *y*-axis in Fig. 11 can be considered to be the equivalent of a time axis. Initially, ($y = 0$) the image is equivalent to that observed at o.c.p. (Fig. 9). As time increases, the image becomes less resolved and the tip current decreases. At short times, the image has good contrast between the Ni and epoxy matrix. This contrast is due to the presence of an O_2 gradient between the epoxy (high O_2) and Ni (less O_2). At longer times ($y > 100$) the image shows less overall current as the O_2 is depleted near the substrate surface by anodic dissolution of the Ni (thus generating a significant Ni^{2+} concentration in the vicinity of the substrate). The region of depleted O_2 extends beyond the Ni-composite surface due to the effect of diffusion. The implication of this result is that O_2 reduction occurs more uniformly across the surface when the Ni substrate is polarized at 100 mV more positive potential (vs. o.c.p.) than when the substrate is floating at the o.c.p. Polarization apparently overcomes local anodic and cathodic activity of the o.c. electrode, eliminating variations in O_2 concentration. The time to acquire the image in Fig. 11 is about 20 min. The fact that the change in image does not occur instantly upon polarization, but evolves slowly is an indication that the net oxygen consumption is small and roughly similar at the polarized and o.c. electrode (Fig. 9). These images also indicate that Ni^{2+} reduction at the tip is not a primary source of the

image contrast. Ni^{2+} reduction would produce an *increase* in cathodic current at the probe electrode. An alternate explanation is that the probe electrode is reducing H^+ ion and thus the decrease in cathodic current is attributed to a local decrease in H^+ ion.[22] This explanation is unlikely since the Pourbaix diagram indicates that the H^+ reduction at Ni is not favored at these potentials. In addition, the magnitudes of the current changes are consistent with the change in probe electrode current at –0.3 V in the absence and presence of O_2 as seen in the CVs of Fig. 8. A final possible explanation is that, due to the consumption of H^+ on the cathodic sites [eq. 3], there is a locally higher concentration of OH^- ions, which react with Ni^{2+} ions to form a nickel hydroxide, covering the Ni surface and causing a local loss of SECM image resolution. This behavior would mask variations in activity at the electrode surface.

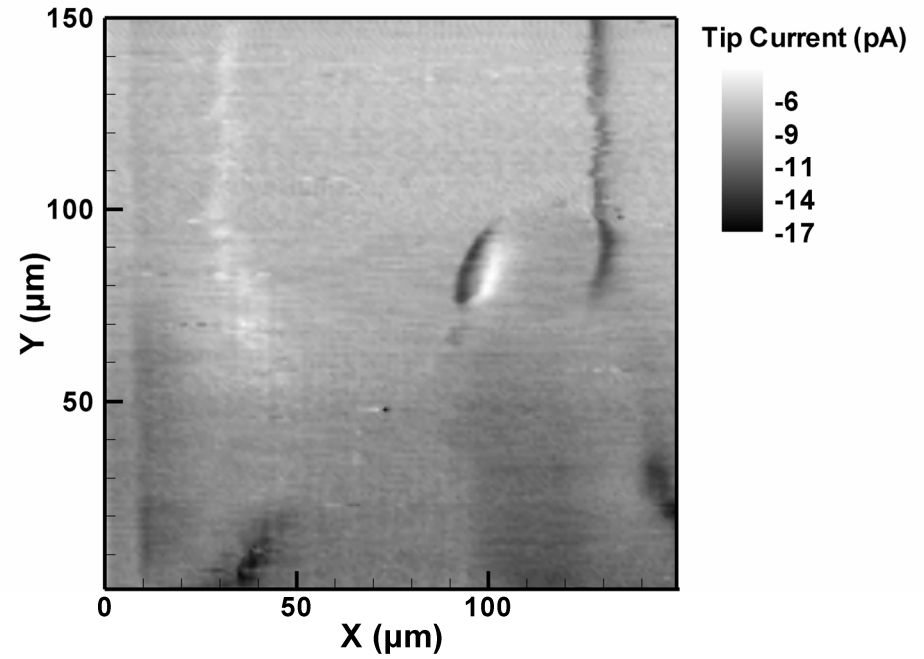

Fig. 11 SECM image of the probe current monitored on Ni-Y_2O_3 composite substrate at an anodic polarization of 100 mV (vs. o.c.p.), in phosphate-citrate buffer at pH 4.2

A vertical concentration map (Fig. 12) provides more evidence of O_2 consumption at the anodic polarized Ni substrate (100 mV vs. o.c.p.). The map is acquired at 50 μm along axis *y* in Fig. 10. The monitored tip current shows a decrease in oxygen concentration when the tip approaches the Ni substrate and the lighter "cloud" defines the thickness of sample and its border with the epoxy substrate. It can be seen that in the bulk of the solution (100 μm over the Ni substrate), the oxygen concentration is ~ 30% higher. This is consistent with the SECM results of Gilbert and coworkers at a titanium surface.[24]

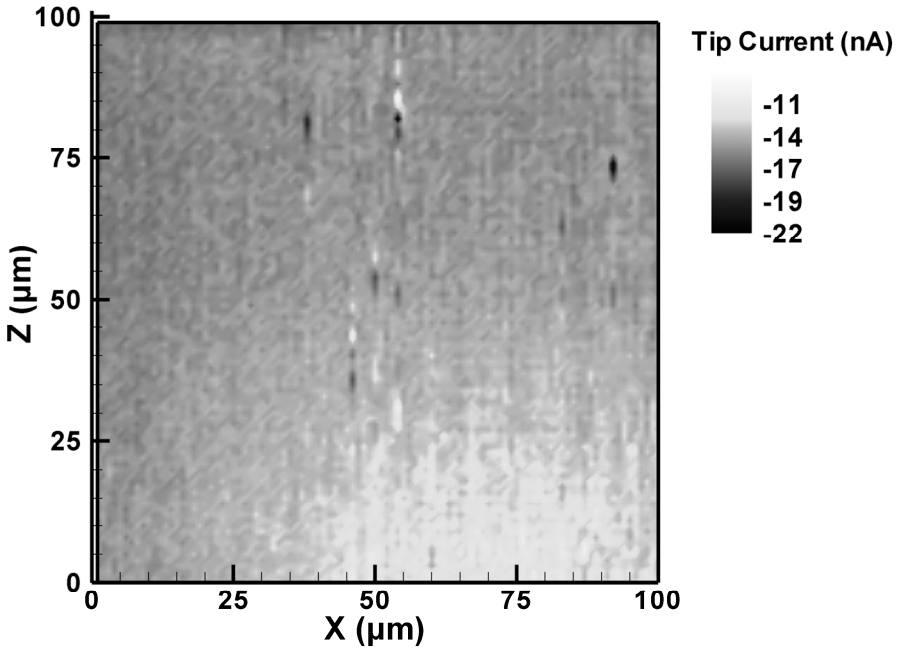

Fig. 12 SECM vertical concentration map of reduction of oxygen on Ni coating substrate (at anodic polarization of 100 mV vs. o.c.p.), in phosphate-citrate buffer at pH 4.2

Conclusions

Electrodeposited nickel and Ni-Y_2O_3 composite samples were compared using *in situ* SECM in mixed feedback and substrate generation-tip collection (SG/TC) modes. The

experiments were done in phosphate-citrate buffer (at pH 4.2) in absence or presence of $Ru(NH_3)_6^{3+}$ as an oxidizing agent (mediator). SECM images with the addition of a mediator clearly indicate regions of higher and lower electrochemical activity on Ni and Ni-composite surface. The SECM images with the presence of a mediator define the shape, activity, and location of particles, such as Y_2O_3 introduced (co-deposited) in the Ni-matrix of the composite. The Ni-matrix in the composite coating appears more active than the pure Ni-coating. This difference is significant when an oxidizing agent is used. The electrochemical activity of heterogeneous metal surface is investigated by using O_2 concentration changes in the absence of an additional mediator in the solution. The rate of reaction for O_2 reduction was found to locally vary at electrodes floating at the open-circuit potential when compared to an electrode potentiostatically polarized at 100 mV more positive than the o.c.p. This behavior suggests that local anode and cathode regions are being observed at the o.c.p. sample. This is intriguing and should be of interest when comparing metallic corrosion data acquired at o.c.p. or potentiostatically.

Acknowledgments

The authors would like to acknowledge the National Science Foundation for support by grant DBI-9987028. L.D. thanks Mexican CONACYT for his sabbatical scholarship during this period. The authors are grateful to T. Muleshkov and N. Muleshkov for their assistance with the deposition of coatings samples and also to Prof. M. Kaisheva for providing an Y_2O_3 sample.

References

1. in *Corrosion, Volume 1: Metal/Environment Reaction*, L. L. Shreir, R. A. Jarman and G. T. Burstein, Editors, p. 340, Butterworth Heinemann, (1994).

2. C. Dedeloudis, M. K. Kaisheva, N. Muleshkov, T. Muleshkov, P. Nowak, J. Fransaer and J. P. Celis, *Plat. Surf. Finish.*, **57**, 57 (1999).

3. P. Nowak, R. P. Socha, M. Kaisheva, J. Fransaer, J. P. Celis and Z. Stoinov, *J. Appl. Electrochem.*, **30**, 429 (2000).

4. A. C. Tavarez and S. Trasatti, *Electrochim. Acta*, **45**, 4195 (2000).

5. M. S. Martín-González, J. García-Jaca, E. Morán and M. Á. Alario-Franco, *J. Mater. Chem.*, **9**, 137 (1999).

6. I. Zhitomirsky and A. Petric, *J. Mater. Chem.*, **10**, 1215 (2000).

7. Y. Matsuda, K. Imahashi, N. Yoshimoto, M. Morita and M. Haga, *J. Alloys Compounds*, **193**, 277 (1993).

8. F. Jollet, C. Noguera, N. Thromat, M. Gautier and J. P. Duraud, *Phys. Rev. B*, **42**, 7587 (1990).

9. R. C. Anderson, in *Refractory Materials 5, High Temperature Oxide, Part II*, A. M. Alper, Editor, p. 1, Academic, New York, (1970).

10. R. K. Wilson, H. L. Flower, G. A., J. Hack and S. Isobe, *Adv. Mat. Processes*, **149**, 19 (1996).

11. J. Xu, B. Xinde, F. Yudian, I. Wenliang and B. Hongbin, *J. Mat. Sci.*, **35**, 6225 (2000).

12. R. Guerrero, Ph.D. Thesis, *Reactive Element Effect (Y2O3) Study for the Protection of ZINALCO Alloy*, Inst. Technology, Tijuana, Mexico, (2001).

13. R. Guerrero, M. Farías and L. Cota-Azaiza, *Appl. Surf. Sci.*, **185**, 248 (2002).

14. L. Veleva, M. Kaisheva, P. Quintana and T. Muleshkov, , .

15. A. J. Bard, in *Scanning Electrochemical Microscopy*, A. J. Bard and M. V. Mirkin, Editors, p. 2, John Wiley & Sons, New York, (2001).

16. K. Fushimi and M. Seo, *Electrochim Acta*, **47**, 121 (2001).

17. C. H. Paik and R. C. Alkire, *J. Electrochem. Soc.*, **148**, B276 (2001).

18. I. Serebrennikova and H. S. White, *Electrochem. Solid State Lett.*, **4**, B4 (2001).

19. K. Fushimi, T. Okawa, K. Azumi and M. Seo, *J. Electrochem. Soc.*, **147**, 524 (2000).

20. J. W. Still and D. O. Wipf, *J. Electrochem. Soc.*, **144**, 2657 (1997).

21. N. Casillas, S. J. Charlebois, W. H. Smyrl and H. S. White, *J. Electrochem. Soc.*, **140**, L142 (1993).

22. K. Jambunathan, B. C. Shah, J. L. Hudson and A. C. Hillier, *J. Electroanal. Chem.*, **500**, 279 (2001).

23. J. L. Gilbert, S. M. Smith and E. P. Lautenschlager, *J. Biomed. Mater. Res.*, **27**, 1357 (1993).

24. J. L. Gilbert, L. Zarka, E. B. Chang and C. H. Thomas, *J. Biomed. Mater. Res.*, **42**, 321 (1998).

25. A. J. Bard, F.-R. F. Fan, J. Kwak and O. Lev, *Anal. Chem.*, **61**, 132 (1989).

26. F. M. Zhou, P. R. Unwin and A. J. Bard, *J. Phys. Chem.*, **96**, 4917 (1992).

27. R. C. Engstrom, T. Meany, R. Tople and R. M. Wightman, *Anal. Chem.*, **59**, 2005 (1987).

28. R. C. Engstrom, M. Weber, D. J. Wunder, R. Burgess and S. Winguist, *Anal. Chem.*, **58**, 844 (1986).

29. B. Aiken and E. Matijevich, *J. Coll. Interface Sci.*, **138**, 645 (1988).

30. G. A. Parks, *Chem. Rev.*, **65**, 177 (1965).

31. C. H. Paik, H. S. White and R. C. Alkire, *J. Electrochem. Soc.*, **147**, 4120 (2000).

32. M. V. Mirkin and B. R. Horrocks, *Anal. Chim. Acta*, **406**, 119 (2000).

33. D. O. Wipf and A. J. Bard, *Anal. Chem.*, **64**, 1362 (1992).

34. G. D. Fasman, in *Practical Handbook of Biochemistry and Molecular Biology*, p. 555, CRC Press, Boca Raton FL, (1992).

35. M. Pourbaix, in *Atlas of Electrochemical Equilibria in Aqueous Solutions*, p. 333, NACE-Cebelcor, Houston, (1974).